Lattice dynamics in the $FeSb_3$ skutterudite

A. Möchel,[1,2] I. Sergueev,[3] N. Nguyen,[4] Gary J. Long,[5] Fernande Grandjean,[2] D. C. Johnson,[4] and R. P. Hermann[1,2,*]

[1]*Jülich Centre for Neutron Science JCNS and Peter Grünberg Institut PGI, JARA-FIT, Forschungszentrum Jülich GmbH, D-52425 Jülich, Germany*

[2]*Faculté des Sciences, Université de Liège, B-4000 Liège, Belgium*

[3]*European Synchrotron Radiation Facility, F-38043 Grenoble Cedex, France*

[4]*Department of Chemistry and Materials Science Institute, University of Oregon, Eugene, Oregon 97403, USA*

[5]*Department of Chemistry, Missouri University of Science and Technology, University of Missouri, Rolla, Missouri 65409-0010, USA*

(Received 1 March 2011; revised manuscript received 4 July 2011; published 19 August 2011)

Thin films of $FeSb_3$ were characterized by electronic transport, magnetometry, x-ray diffraction, ^{57}Fe and ^{121}Sb nuclear inelastic scattering, and ^{57}Fe Mössbauer spectroscopy. Resistivity and magnetometry measurements reveal semiconducting behavior with a 16.3(4) meV band gap and an effective paramagnetic moment of 0.57(6) μ_B, respectively. A systematic comparison of the lattice dynamics with $CoSb_3$ and $EuFe_4Sb_{12}$ reveals that the Fe_4Sb_{12} framework is softer than the Co_4Sb_{12} framework, and that the observed softening and the associated lowering of the lattice thermal conductivity in the RFe_4Sb_{12} filled skutterudites are not only related to the filler but also to the Fe_4Sb_{12} framework.

DOI: 10.1103/PhysRevB.84.064302 PACS number(s): 63.20.D−, 76.80.+y, 72.20.Pa, 61.05.C−

I. INTRODUCTION

Skutterudites are promising thermoelectric materials that have been intensively studied since the 1990s.[1–4] They possess interesting semiconducting properties, notably a large Seebeck coefficient, and a relatively low thermal conductivity that has been ascribed to the dynamics of the filler.[5–7] In particular the lattice dynamics of filled and unfilled skutterudites has been the object of intensive research.[8–12] The semiconducting, magnetic, and thermal properties of the filled $R(Fe,Co)_4Sb_{12}$ skutterudites can be tuned[6,13] by filling the $(Fe,Co)_4Sb_{12}$ framework with monovalent ions (e.g., Na^+ and Tl^+), divalent ions (e.g., Yb^{2+} and Eu^{2+}), or trivalent ions (e.g., La^{3+} and Ce^{3+}). However, only a limited degree of filling can be achieved[6,13,14] in $CoSb_3$. In order to achieve larger degrees of filling, either Co must be substituted by Fe or a synthesis involving ball milling and subsequent hot pressing must be used.[15]

Because there is no successful bulk synthesis procedure, the influence of filling the $FeSb_3$ structure on its lattice dynamics has been studied using different approaches. The direct comparison with the lattice dynamics of the Fe_4Sb_{12} polyanion is not possible, thus one approach is the comparison[9,10] of the lattice dynamics of the filled structures mentioned above with the related unfilled $CoSb_3$. Another approach is the study of the contribution of the filler R to the density of phonon states (DPS). Density functional theory calculations of the partial density of phonon states have been carried out and compared with experimental data obtained by inelastic neutron scattering and nuclear inelastic scattering.[16,17] The partial contributions to the DPS can also be investigated by *ab initio* powder-averaged lattice dynamic calculations and a subsequent comparison with inelastic neutron scattering measurements.[11]

The synthesis of $FeSb_3$ is, however, possible by nanoalloying[18,19] and this approach has recently been improved and now yields higher sample purity, but still produces only small amounts in the form of micrometer-thick films. Because detailed knowledge of the lattice dynamics in skutterudites is necessary to unravel the mechanisms that yield their low thermal conductivity, characterization methods suitable for thin films have to be used. Although inelastic neutron scattering experiments are in principle feasible, the beam time required would be prohibitively long because of the small amount of sample. In contrast, nuclear inelastic scattering (NIS) is a method of choice that yields the DPS for selected elements[20] even with small samples. This method has been applied[21] to the ^{57}Fe nuclear resonance for some time, and has recently been developed[17] for the ^{121}Sb resonance. The resolution for the latter isotope was recently improved[22] to ∼1.3 meV full width at half maximum (FWHM). It is thus possible to fully access the element-specific DPS in $FeSb_3$ and to obtain several related quantities,[20] such as the mean force constants, the atomic displacement parameters, and the average velocity of sound.

Herein we report both the macroscopic characterization of high-purity $FeSb_3$ using resistivity and susceptibility measurements, and the microscopic characterization using synchrotron radiation diffraction, ^{57}Fe Mössbauer spectral measurements, and nuclear inelastic scattering by ^{57}Fe and ^{121}Sb. A comparison of these results with the properties of $CoSb_3$ reveals that $FeSb_3$ is significantly softer, which is an observation that both indicates a combined influence of the filler and the substitution of Fe for Co on the lattice dynamics and hence thermal properties, and provides additional clues to the low thermal conductivity in filled skutterudites.

II. EXPERIMENT

The $FeSb_3$ thin films were deposited on Kapton foil at ambient temperature by the elemental modulated reactant method in a custom-built, ultra-high vacuum (≈10^{-5} Pa) deposition system described elsewhere.[23] Fe was deposited using a 3 kW electron-beam gun at a rate of 0.4 Å/s, and Sb was deposited using an effusion cell at a rate of 0.6 Å/s. A computer was used to control the deposition procedure. A quartz-crystal monitoring system placed 25 cm above each source was used to

control the elemental layer modulation, the deposition rates, the shutter opening time for Fe, and the thickness for Sb. The precursors for the crystallized films were prepared by depositing multiple alternate layers of Fe and Sb until the desired film thickness was obtained. Deposition parameters were determined to yield the appropriate molar stoichiometry of $FeSb_3$. These precursor films were then annealed under a nitrogen atmosphere at 410 K to form $FeSb_3$. With this method, two films of thicknesses of ∼1 and ∼1.5 μm were deposited on a 25-μm-thick Kapton substrate. All further measurements were carried out on these two films.

Temperature-dependent resistivity and magnetization measurements were carried out between 10 and 300 K on a Quantum Design physical-properties measurement system (QD-PPMS) with the resistivity and the vibrating sample magnetometer options. The resistivity was measured on several 1-μm-thick samples with 2 by 5 mm^2 lateral dimensions and different microcrack structures using the four-point method. The magnetization measurements were carried out with an applied magnetic induction of 0.25 T on a wrapped ribbon of the 1-μm-thick film that was 80 cm by 3.7 mm, i.e., ∼12.9 mg of $FeSb_3$. Hysteresis measurements have been carried out at 300 K up to 1.5 T in order to assess the presence of impurity phases and the diamagnetic contribution to the susceptibility. The same measurements have been carried out on polycrystalline $CoSb_3$ for comparison. The susceptibility χ was calculated from the magnetization by assuming the validity of the low field limit approximation $\chi = M/H$, where M is the magnetization and H is the applied field.

Temperature-dependent x-ray diffraction (XRD) measurements were carried out at the 6-ID-D high-energy station at the Advanced Photon Source between 10 and 300 K. The x-ray wavelength was 0.124269 Å, and the sample-area detector distance was 1601.1(1) mm, as determined with a NIST SRM640c Si standard. Silicon (Chempur, 99.999%) was used as an internal standard for the temperature calibration. The sample contained ten layers of a ∼1.5-μm-thick film of $FeSb_3$ on Kapton foil and, for better thermal coupling to the sample holder, Al foil was placed between each layer. The powder-diffraction pattern of $CoSb_3$ was measured under the same conditions. The data were reduced to diffractograms by using FIT2D[24] and analyzed using the Rietveld method.[25]

The ^{57}Fe Mössbauer spectra have been measured between 4.2 and 295 K on a constant-acceleration spectrometer that utilized a 295 K rhodium-matrix ^{57}Co source and was calibrated at 295 K with α-Fe powder.

The ^{121}Sb NIS by $FeSb_3$ was measured at the ID22N station at the European Synchrotron Radiation Facility (ESRF) operating in 16-bunch mode. A resolution of 1.3 meV was achieved by using a high-resolution backscattering monochromator with the (8 16 $\overline{24}$ 40) reflection of a sapphire single crystal cooled to ∼237 K. The sample containing six layers of a ∼1.5-μm-thick film of $FeSb_3$ on Kapton foil with Al foil between each layer was cooled to 25 K in order to minimize multiphonon scattering. The ^{121}Sb NIS of $CoSb_3$ and $EuFe_4Sb_{12}$ was measured on powder samples with the same setup and resolution. The 295 K ^{57}Fe NIS on the same $FeSb_3$ sample was measured at the ID18 station at the ESRF operating in 16-bunch mode with a resolution of 0.7 meV.

III. RESULTS AND DISCUSSION

A. Electric transport and magnetism

Above ∼40 K, the electrical resistivity ρ_{el} of $FeSb_3$ decreases with increasing temperature (see Fig. 1), a decrease that is indicative of semiconducting behavior. A fit of the data in the high-temperature region (see inset in Fig. 1) with[26] $\rho_{el}(T) = A[\exp(E_g/(2k_BT))]$, where E_g is the energy gap, k_B is the Boltzmann constant, T is the temperature, and A is a proportionality constant, yields an electronic band gap of 16.3(4) meV, which is a narrower gap than the 50 meV gap obtained by resistivity measurements[26] on lightly p-doped $CoSb_3$. As expected for rather thin films, the microstructure was found to be very important and resistivity measurements were carried out on several samples. The smallest cracks or scratches increase the resistivity by several orders of magnitude with respect to pristine samples. Further, heating the sample above 300 K (not shown) induces additional microstructure and increases the resistivity because of the differential thermal expansion between Kapton and $FeSb_3$. Atomic-force microscopy measurements were carried out to monitor this behavior and to assure that the results in Fig. 1 were obtained on a sample free of cracks at the ∼50 nm level. Such a dependence of the resistivity on the microstructure has also been observed[27] in polycrystalline $CoSb_3$, with reported resistivities of undoped samples between 7 and 1000 $\mu\Omega$m at room temperature.[27–33] The 300 K resistivity of 29.4(1) $\mu\Omega$m observed for crack-free $FeSb_3$ is similar to the 37 $\mu\Omega$m of a polycrystalline, sintered, $CoSb_3$ sample,[30] which also exhibits the temperature dependence of a typical semiconductor.

The molar susceptibilities χ_m of $FeSb_3$ and $CoSb_3$ are shown in Fig. 2. First, the diamagnetic contribution was obtained from the slope of a hysteresis loop measurement at 300 K (see Fig. 3) and associated with the sample holder, the ion core diamagnetism, and, for the $FeSb_3$ films, with the Kapton substrate. The resulting corrections of χ_m^{dia} were assumed to be temperature independent and were used to obtain the results shown in Fig. 2. Second, a small amount of soft ferromagnetic impurity in $FeSb_3$ was observed in the hysteresis

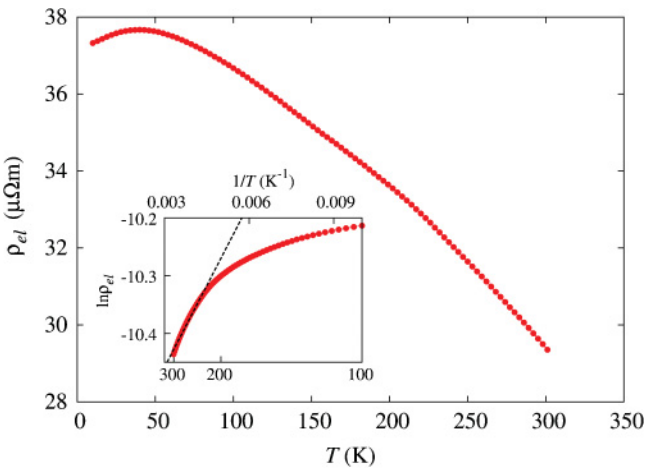

FIG. 1. (Color online) Electrical resistivity ρ_{el} of $FeSb_3$ obtained between 10 and 300 K on a crack-free sample; the errors are the size of the data points. The inset shows the fit between 220 and 300 K that yields an energy gap of 16.3(4) meV; see text.

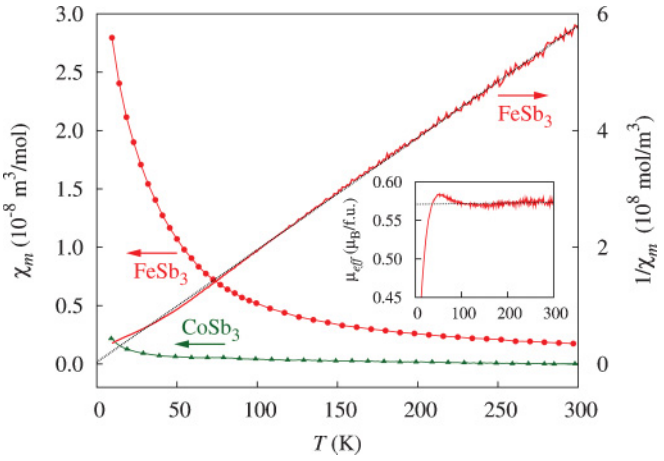

FIG. 2. (Color online) The molar magnetic susceptibility and the inverse susceptibility obtained at 0.25 T between 10 and 300 K for $FeSb_3$ shown as red circles, and the molar magnetic susceptibility for $CoSb_3$ shown as green triangles, after corrections; see text. The errors are the size of the data points. Inset: the effective magnetic moment of $FeSb_3$.

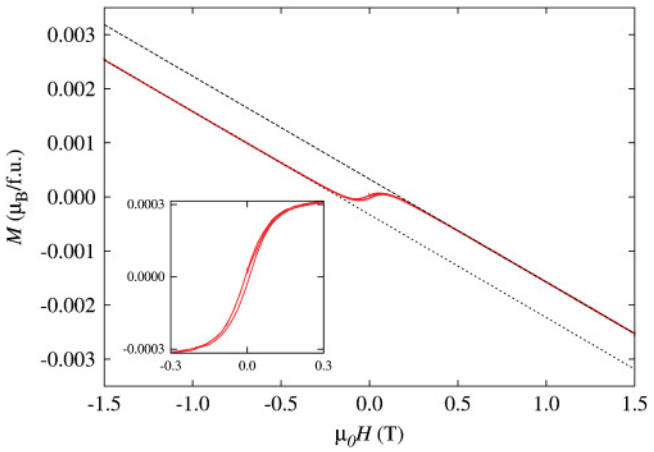

FIG. 3. (Color online) Hysteresis loop of $FeSb_3$ measured at 300 K. The negative slope is indicative of diamagnetic behavior. The inset shows the hysteresis loop obtained after the diamagnetic correction that is discussed in the text.

loop (see Fig. 3), and this contribution was subtracted. The magnetization of this impurity is essentially saturated at 0.25 T. Finally, a small correction term χ_0, amounting to $\sim$12% of the diamagnetic correction, was added to account for imperfections in the correction procedure. Adding χ_0 immediately yielded paramagnetic Curie-Weiss behavior for $FeSb_3$ between 70 and 300 K. A plot of $1/\chi_m$ (see Fig. 2) yields a Curie constant of 0.520(2) cm^3 K/mol with a Curie-Weiss temperature of 0 K. The inset of Fig. 2 indicates that the effective paramagnetic moment of $FeSb_3$ of 0.57(6) μ_B/f.u., obtained from $\mu_{\text{eff}} = 797.8\sqrt{\chi_m T}$, is temperature independent above $\sim$70 K. The same approach was used for $CoSb_3$ and an effective paramagnetic moment of 0.10(6) μ_B/f.u. was obtained, a value that is compatible with an earlier report.[33] A study of $Co_{1-x}Fe_xSb_3$, with x ranging from 0 to 0.1, has shown that μ_{eff} increases with increasing Fe content up to a maximum of 1.7 μ_B/f.u., a value that could correspond[32] to low-spin Fe^{3+}. This behavior obviously does not extrapolate to $FeSb_3$, which exhibits a much smaller effective paramagnetic moment.

From the y-axis intercept of the magnetic hysteresis loop in Fig. 3, an impurity phase of 0.004(1) at. % was obtained by assuming a typical mean value of 2.2 μ_B per Fe impurity atom at room temperature. The coercive field of $\sim$80 Oe indicates that the impurity phase is not elemental Fe. For $CoSb_3$, an elemental Co impurity phase of 0.0005(2) at. % was obtained using the same procedure.

B. X-ray diffraction

X-ray diffraction (see Fig. 4) indicates[18,34] that both $FeSb_3$ and $CoSb_3$ form a cubic lattice with space group $Im\bar{3}$ (No. 204) and have the skutterudite structure (see Fig. 5), where Fe or Co and Sb are located on the 8c and 24g sites, respectively. The inset to Fig. 4 shows the detector image with homogeneous Debye-Scherrer rings that indicate the absence of texture. Apart from the Si internal standard, small traces of an impurity are observed as a shoulder at $2\theta \sim 2.3^\circ$ in Fig. 4, indicating a polycrystalline Sb impurity of less than 3 wt. %. No further phases or Al thermalization layers are observed. Because of the large background resulting from the ten layers of Kapton foil, the Fourier filtering option was used to properly subtract the background, however, even with this option, the data below $2\theta = 2.1^\circ$ cannot be refined because the background is too large and not monotonous. The parameters obtained at 10 and 300 K using Rietveld refinements are given in Table I. The Sb occupation was refined assuming full occupation of the Fe or Co site. The density obtained from the lattice parameters is also given in Table I. A temperature-dependent diffraction study on $CoSb_3$ was carried out for comparison and the refinement parameters given in Table I are in good agreement with the literature values.[34] From the refinement of the Sb occupation at 10 K, a stoichiometry of $FeSb_{2.88(5)}$ and $CoSb_{2.97(3)}$ has been obtained. The corresponding 0.96(1) Sb occupancy in $FeSb_3$ is, however, problematic; see discussion in Sec. III C.

A study of the $Co_{1-x}Fe_xSb_3$ solid solutions, with x between 0 and 0.1, reveals that their lattice parameter increases linearly with increasing Fe content, which is in agreement with Vegard's law.[32] If we assume that this linearity holds true for higher Fe content, then a lattice parameter of 9.126 Å is expected for $FeSb_3$, a value that is in clear disagreement with the much larger 9.2383(6) Å found herein at 300 K.

TABLE I. Rietveld refinement parameters for $FeSb_3$ and $CoSb_3$.

	$FeSb_3$ (10 K)	$FeSb_3$ (300 K)	$CoSb_3$ (300 K)
Bragg R factor (%)	7	6	6
R_f (%)	6.5	6.5	5
a (Å)	9.2116(6)	9.2383(6)	9.0320(8)
y Sb	0.3402(2)	0.3399(3)	0.3356(3)
z Sb	0.1578(2)	0.1573(3)	0.1586(3)
Sb occupation (%)	0.96(1)	0.96(1)[a]	0.99(1)[a]
Density (g/cm^3)	7.157(1)	7.096(1)	7.648(1)
$\langle u^2 \rangle$ Sb (Å^2)	0.028(1)	0.034(1)	0.004(1)
$\langle u^2 \rangle$ Fe/Co (Å^2)	0.010(3)	0.013(3)	0.011(3)

[a]constrained to the 10 K value.

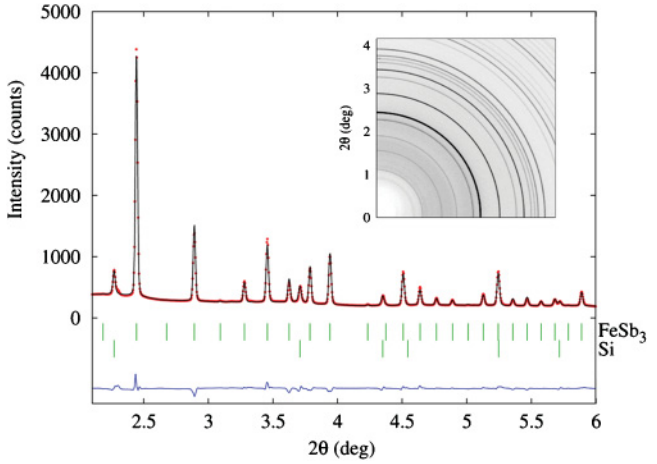

FIG. 4. (Color online) X-ray diffraction pattern of $FeSb_3$ obtained at 10 K (red dots), the corresponding Rietveld refinement (black line), the difference plot (blue line), and the peak positions for $FeSb_3$ and Si (green ticks). Inset: A quarter of the corresponding detector image.

The thermal expansion calculated from the temperature dependence of the lattice parameters is shown in Fig. 6. In order to reduce noise in the data, especially at low temperatures, the temperature dependence of the lattice parameters was first modeled with a third-order polynomial function $a_m(T)$; see the fit lines at the top of Fig. 6. The differences between the fitted curve and the data were less than 4×10^{-4} Å. The thermal expansion coefficient α was then obtained from the derivative, $\alpha = [da_m(T)/dT]/a_m(300\ \mathrm{K})$. The thermal expansion coefficient of $CoSb_3$ at 220 K of $8.8\times10^{-6}\ \mathrm{K}^{-1}$ is in good agreement with the literature value[35] of $9.1\times10^{-6}\ \mathrm{K}^{-1}$, as obtained from dilatometry. The thermal expansion of $FeSb_3$ is larger compared to $CoSb_3$. Under the assumption that Poisson's ratio for $CoSb_3$ (Ref. 9), $\nu = 0.22$, is the same for $FeSb_3$, the bulk modulus can be extracted from the sound velocity,[36] which can be obtained from NIS; see below. The Grüneisen coefficient[37] $\gamma = 3\alpha B V_m/C_V$ can be obtained using the thermal expansion coefficient, the bulk modulus $B = 47.9(1)$ and 83.2(1) GPa for $FeSb_3$ and $CoSb_3$, respectively, the molar volume V_m, and the heat capacity C_V; see below. In $FeSb_3$, the resulting γ value of 1.4(1) at 300 K is only slightly larger than the 1.30(5) obtained for $CoSb_3$ because $FeSb_3$ exhibits both a much larger thermal expansion and a much smaller bulk modulus as compared to $CoSb_3$.

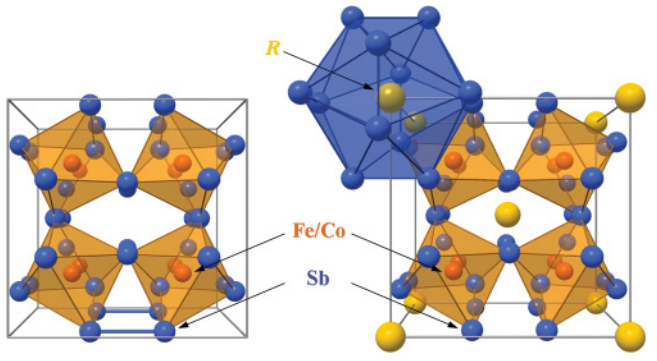

FIG. 5. (Color online) The structure of unfilled $CoSb_3$ or $FeSb_3$ (left) and filled RFe_4Sb_{12} (right) skutterudite. Co or Fe, Sb, and R are shown in red, blue, and yellow, respectively. The blue rectangle indicates one of the Sb rings; see text.

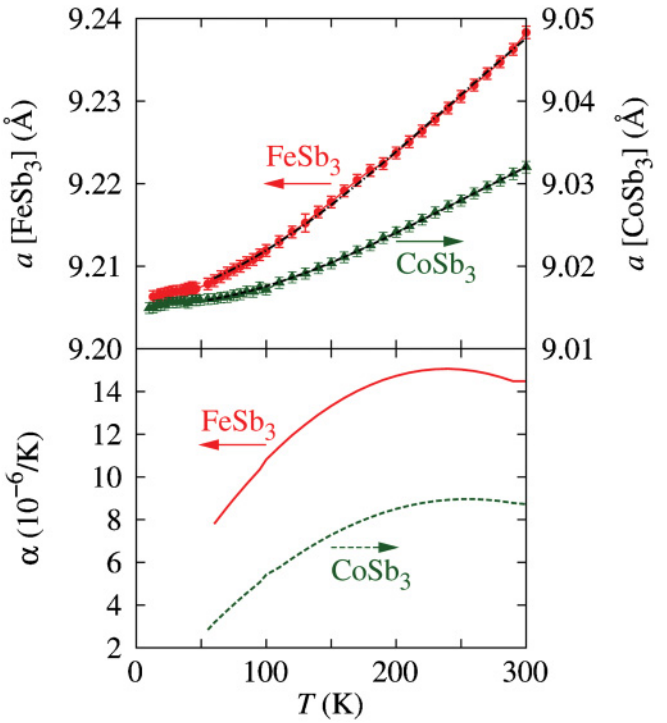

FIG. 6. (Color online) Top: The temperature dependence of the lattice parameter a for $FeSb_3$ (red) and $CoSb_3$ (green), and the corresponding polynomial fit (black). Bottom: The thermal expansion coefficient α of $FeSb_3$ and $CoSb_3$.

The isotropic mean-square displacements $\langle u^2\rangle$ were refined for $FeSb_3$ and $CoSb_3$; see Table I. The absolute values for the Sb mean-square displacements are not reliable because they are too large for $FeSb_3$, whereas for $CoSb_3$, they are too small with respect to an expected value of ∼0.01 Å^2 at 300 K; see Sec. III D. The likely reason for this discrepancy is that the 2θ range of the measurement was too narrow. Nevertheless, the temperature dependence of the mean-square displacements is reasonable. From the slope,[38] $d\langle u^2\rangle/dT = 3\hbar^2/(m k_B \theta_D^2)$, where m is the mass of Sb, Fe, or Co, fitted between 100 and 300 K, Debye temperatures θ_D of 230(5) and 410(10) K for Sb and Fe, respectively, have been obtained for $FeSb_3$. The average value of the Debye temperature in $FeSb_3$, calculated from $\theta_D^{\mathrm{av}} = (3\theta_{D,\mathrm{Sb}} + \theta_{D,\mathrm{Fe/Co}})/4$, is 275(5) K. In $CoSb_3$, the Debye temperatures of 280(10) and 380(30) K for Sb and Co, respectively, have been obtained, and $\theta_D^{\mathrm{av}} = 305(15)$ K is larger than in $FeSb_3$; the average value is in good agreement with the literature value[39] of 307 K obtained from the heat capacity of $CoSb_3$.

Sb is located on a general $(0, y, z)$ position and the y and z positions have been refined. $y + z = 0.4972(6)$ and 0.4942(6) for $FeSb_3$ and $CoSb_3$, respectively. $FeSb_3$ more closely fulfills the Oftedal relation[40] $y + z = 1/2$, which indicates that the rectangular Sb rings (see Fig. 5) are closer to squares in $FeSb_3$ than in $CoSb_3$.

C. Mössbauer spectroscopy

The 4.2 and 295 K ^{57}Fe Mössbauer spectra of the ∼1.5 μm film of $FeSb_3$ are shown in the upper panel of Fig. 7; the spectra

TABLE II. Mössbauer spectral parameters for the $FeSb_3$ films. The errors are estimated to be 0.005 mm/s for the isomer shift δ, quadrupole splitting ΔE_Q, and linewidth Γ, and 0.005% ϵ (mm/s) for the absorption area.

Thickness (μm)	T (K)	δ (mm/s)[a]	ΔE_Q (mm/s)	Γ (mm/s)	Total area (%ϵ) (mm/s)
1	295	0.390	0.338	0.297	1.668
	225	0.432	0.350	0.302	1.798
	155	0.463	0.363	0.307	1.917
	85	0.490	0.373	0.309	2.029
	60	0.491	0.379	0.306	2.037
	30	0.494	0.375	0.306	2.040
	4.2	0.493	0.375	0.315	2.070
1.5	295	0.389	0.333	0.276	2.808
	225	0.432	0.347	0.293	3.045
	155	0.465	0.366	0.309	3.266
	85	0.490	0.373	0.312	3.471
	60	0.489	0.375	0.303	3.526
	30	0.490	0.373	0.312	3.577
	4.2	0.493	0.375	0.312	3.564

[a]The isomer shifts are given relative to 295 K α-Fe powder.

obtained for both films and at intermediate temperatures are very similar. In addition to the diffraction measurements that revealed no crystalline impurity phase, no further amorphous iron-bearing impurity is observed. All measured spectra were fitted with a simple symmetric quadrupole doublet with two Lorentzian line shapes, with parameters given in Table II. The Mössbauer spectra show no convincing evidence for a second component related to Fe with missing Sb near neighbors, as would be expected from the hypothetical partial Sb occupancy seen in the diffraction measurements. The 96(1)% Sb occupancy (see Table I) would imply that more than 20% of the Fe have less than six Sb near neighbors, which would be visible in the Mössbauer spectra. The temperature dependence of the isomer shift δ, quadrupole splitting ΔE_Q, linewidth Γ, and the recoil-free fraction $f_{\rm LM}$ are shown in the lower panel of Fig. 7. The temperature dependence of δ and $f_{\rm LM}$ have been fit with a Debye model for a solid.[41]

The temperature dependence of the isomer shift is well fit with the Debye model[42] for the second-order Doppler shift with a characteristic Mössbauer temperature θ_M of 541(10) and 530(10) K for the ~1.5 and ~1 μm films, respectively. This temperature is much larger than the Debye temperature $\theta_{D,\rm Fe}$ of 350(5) and 373(6) K of the ~1.5 and ~1 μm films, respectively, obtained from the temperature dependence of the logarithm of the spectral absorption area $f_{\rm LM}$. The latter values are in good agreement with the values obtained herein by other techniques; see Table III. It is known[42] that the two temperatures θ_M and $\theta_{D,\rm Fe}$, obtained from the two temperature dependencies, are usually different because they depend, for the isomer shift, on $\langle v^2\rangle$, which is the mean-square vibrational velocity of the ^{57}Fe, and, for the absorption area, on $\langle u^2\rangle$, which is the mean-square atomic displacement of the ^{57}Fe; there is no model-independent relationship between these mean-square values.[42] However, measurements of the Mössbauer temperatures on various compounds[43] indicate that θ_M is often twice as large as $\theta_{D,\rm Fe}$, i.e., the isomer shift is more sensitive to higher-energy phonons.

The Fe DPS of $FeSb_3$ (see below) clearly reveals that the Fe vibrations have a strong non-Debye behavior and are dominated by two strong optical modes above 30 meV. Because we have measured the partial DPS $g(E)$ by ^{57}Fe NIS (see

TABLE III. Summary of the Debye temperatures, sound velocities, and mean force constants in $FeSb_3$ and $CoSb_3$ obtained by different techniques.

	$FeSb_3$			$CoSb_3$		
Technique	$\theta_{D,\rm Sb}$(K)	$\theta_{D,\rm Fe}$(K)	$\theta_D^{\rm av}$(K)	$\theta_{D,\rm Sb}$(K)	$\theta_{D,\rm Co}$(K)	$\theta_D^{\rm av}$(K)
$\langle u^2\rangle$, XRD	230(5)	410(10)	275(5)[a]	280(10)	380(30)	305(15)[a]
Mössbauer spectral area 1.5 μm		350(5)				
Heat capacity DPS	210(5)	430(10)	240(10)	250(5)	410(10)[b]	285(10)
Heat capacity macroscopic						280(10)
DPS	210(10)	370(5)	255(5)[a]	245(5)	360(10)[b]	270(10)[a]
θ_D from v_s			245(5)			307[c]
	$v_{s,\rm Sb}$ (m/s)	$v_{s,\rm Fe}$ (m/s)	$v_s^{\rm av}$ (m/s)	$v_{s,\rm Sb}$ (m/s)	$v_{s,\rm Co}$ (m/s)	$v_s^{\rm av}$ (m/s)
NIS, Debye level	2400(100)	2390(10)		2600(100)		
Pulse echo						2930[d]
	$F_{\rm Sb}^m$ (N/m)	$F_{\rm Fe}^m$ (N/m)		$F_{\rm Sb}^m$ (N/m)	$F_{\rm Co}^m$ (N/m)	
NIS	105(5)	186(1)		160(10)		
Theory				119[b]	176[b]	

[a]obtained from $\theta_D^{\rm av} = [3\theta_{D,\rm Sb} + \theta_{D,\rm Fe/Co}]/4$.
[b]obtained from Ref. 16.
[c]obtained from Ref. 39.
[d]obtained from Ref. 28.

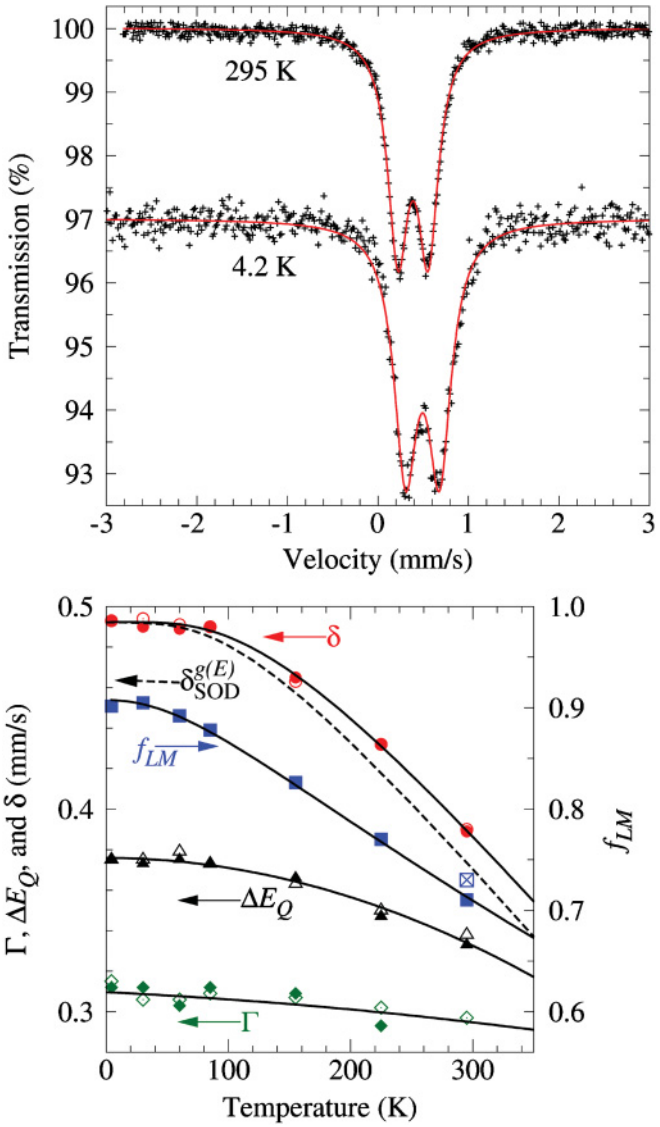

FIG. 7. (Color online) Top: The Mössbauer spectra of $FeSb_3$ obtained on a 1.5 μm film. Bottom: The fit parameters obtained from the spectra of the ∼1 and ∼1.5 μm films (open and closed symbols), respectively. The errors are the size of the symbols. The crossed square indicates the f_{LM} obtained directly from the ^{57}Fe NIS at 295 K. The dashed line indicates the second-order Doppler shift obtained from the DPS; see text. The lines for the Doppler shift and f_{LM} are Debye model fits.[41] The lines for ΔE_Q and Γ are quadratic polynomial fits given as a guide for the eye.

below), we can directly obtain the second-order Doppler shift[42] $\delta_{SOD}^{g(E)} = -\langle v^2\rangle/(2c)$ from the average kinetic energy[20] $\langle E_{kin}\rangle = 1/2 m_R \langle v^2\rangle = 3/4 \int_0^\infty \coth[E/(2k_BT)]g(E)EdE$, where m_R is the mass of the resonant nucleus. The obtained temperature dependence of the isomer shift with the second-order Doppler correction is shown in Fig. 7, and corresponds to θ_M = 440 K. The difference is thus only partly explained and other corrections such as thermal expansion, which modifies the DPS and therefore $\langle E_{kin}\rangle$, or the influence of charge carrier activation on the isomer shift, might be necessary.

D. Nuclear resonance scattering

The nuclear inelastic scattering spectra from the ^{121}Sb NIS measurements in $FeSb_3$, $CoSb_3$, and $EuFe_4Sb_{12}$ are shown in Fig. 8, together with the instrumental functions measured by nuclear forward scattering. The resolution of the instrument was ∼1.3 meV for all measurements. ^{121}Sb NIS measurements on the latter two compounds have been published previously[17] with a resolution of 4.5 meV. The measurements have been repeated because of the enhanced resolution.[22] After subtraction of the elastic peak, the extraction of the DPS has been performed by the conventional procedure,[21,44] i.e., the correction of the multiphonon contribution of the Fourier transformation of the inelastic scattering, which was slightly modified in order to take into account the asymmetry of the instrumental function; the data were deconvoluted by the experimental instrumental function and convoluted with a symmetric Gaussian with a FWHM of 1.7 meV, which is a value slightly larger than the ∼1.3 meV resolution that was chosen in order to avoid unphysical termination ripples in the DPS. The validity of the procedure was confirmed by applying the usual sum rules.[45] The ^{57}Fe NIS spectrum of $FeSb_3$ measured at 295 K is also shown in Fig. 8. The instrumental

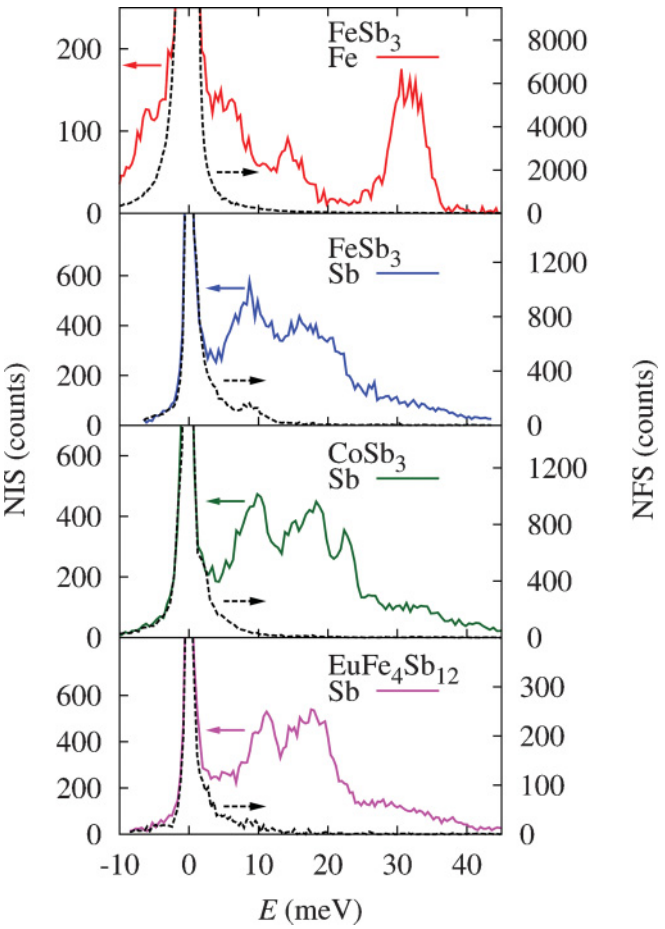

FIG. 8. (Color online) The nuclear inelastic scattering (NIS) spectra and the instrumental functions (dashed lines) measured by nuclear forward scattering (NFS) obtained with the ^{57}Fe resonance of $FeSb_3$ (top graph) and with the ^{121}Sb resonance of $FeSb_3$, $CoSb_3$, and $EuFe_4Sb_{12}$ (bottom three graphs).

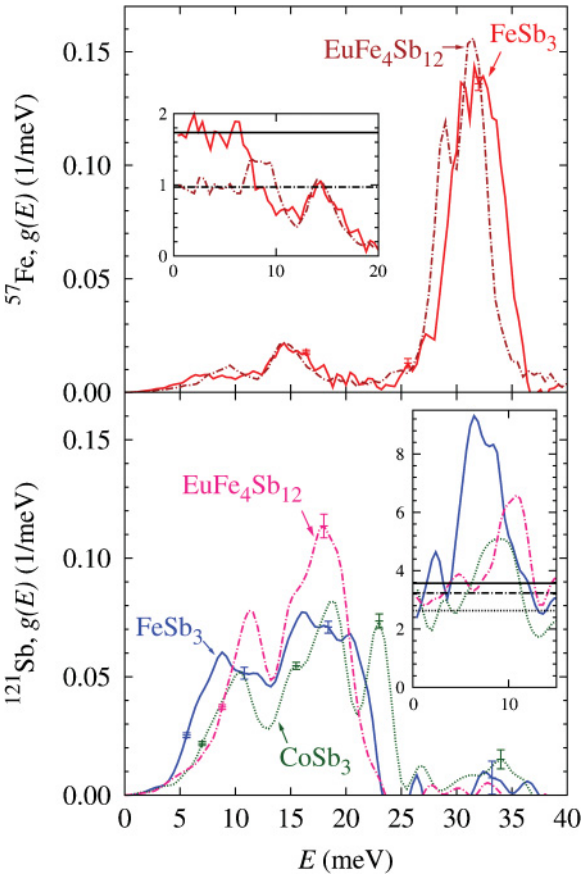

FIG. 9. (Color online) Comparison of the DPS measured with the ^{57}Fe resonance at 295 K for $FeSb_3$ and $EuFe_4Sb_{12}$ (top) and with the ^{121}Sb resonance at 25 K for $FeSb_3$, $CoSb_3$, and $EuFe_4Sb_{12}$ (bottom). The insets show the reduced partial DPS $g(E)/E^2$ in units of 10^{-4}/meV^3, and the low-energy fit between 0 and 4 meV for the Debye levels, indicated by the same type of lines. The differences in the Debye levels for Fe and Sb in $FeSb_3$ and $EuFe_4Sb_{12}$ are due to the different masses of the elements; see Eq. (1).

resolution was 0.7 meV and the DPS was obtained by the conventional procedure.[44] After the multiphonon correction, the partial DPS $g(E)$ were obtained (see Fig. 9), which also shows the ^{57}Fe DPS of $EuFe_4Sb_{12}$ from Ref. 46. The Fe DPS consists of two small broad peaks at ∼7 and 15 meV and a large broad peak around 30 meV. The latter broad peak is split and corresponds to a somewhat softer phonon mode in the $EuFe_4Sb_{12}$ filled skutterudite. The splitting of this peak was also observed in the $LaFe_4Sb_{12}$ filled skutterudite using inelastic neutron scattering measurements,[16] and in $CeFe_4Sb_{12}$ using NIS.[46] The low-energy portion of the DPS indicates that $FeSb_3$ is softer than $EuFe_4Sb_{12}$, as seen from the large increase in the reduced DPS $g(E)/E^2$; see insets to Fig. 9. The Sb vibrations mainly appear below 25 meV, but a small contribution of the Sb vibrations is also observed around 30 meV. The latter part of the DPS is not well resolved due to the multiphonon contributions in the experimental data. By comparing the partial DPS in different compounds, we observe that the Sb DPS in $CoSb_3$ exhibits pronounced features, such as gaps at 12 and 21 meV, and a well-resolved peak at 23 meV. Inelastic neutron scattering measurements have also revealed[16] this better resolution of the individual peaks in $CoSb_3$ as compared with RFe_4Sb_{12}. However, this difference is not directly related to the filling of the skutterudites, because the DPS of $FeSb_3$ shows the same broad features as $EuFe_4Sb_{12}$. The most pronounced difference of the DPS in $FeSb_3$ as compared to other filled and unfilled skutterudites is an overall softening of the phonon modes, which leads to an enhancement of the DPS between 5 and 10 meV. This softening, which is also observed in the Fe DPS in $FeSb_3$ at low energies (see Fig. 9) indicates a lower velocity of sound and might be crucial in determining the thermal conductivity and, therefore, the thermoelectric properties of skutterudites. In $EuFe_4Sb_{12}$, the essentially single frequency and Einstein-like DPS of the Eu filler appears[46] at ∼7 meV. The relative hardening of the Sb DPS between $FeSb_3$ and $EuFe_4Sb_{12}$, seen in the lower DPS of $EuFe_4Sb_{12}$ at ∼7 meV, might be related to the appearance of this filler mode. Calculations of the lattice dynamics in $FeSb_3$ would thus be highly desirable in order to confirm this hypothesis.

Several thermodynamic and vibrational quantities can be obtained from the DPS.[20] The element-specific heat capacity C_V can be directly calculated from the DPS. The total heat capacity $C_V^{\rm tot}$ of $FeSb_3$, obtained by combining the partial C_V for Fe and Sb obtained from NIS by $C_V^{\rm tot} = 3C_V^{\rm Sb} + C_V^{\rm Fe}$, are shown in Fig. 10. These values are compared with the total C_V of $CoSb_3$, obtained by combining the partial C_V for Co obtained from calculations[16] and Sb from NIS measurements, which are measurements that are in good agreement with the calculation in Ref. 16. A macroscopic C_P measurement of $CoSb_3$, carried out with the C_P option of the QD-PPMS that is in excellent agreement with earlier results,[39] is also shown. With a Debye fit of the C_V between 2 and 300 K, Debye temperatures for Sb and Fe in $FeSb_3$ of 210(5) and 430(10) K, respectively, have been obtained, values that are in good agreement with those obtained by diffraction; see Table III. From $C_V^{\rm tot}$ for $FeSb_3$, a Debye temperature of 240(10) K has been obtained. The partial C_V of $CoSb_3$ yields Debye temperatures of 250(5) and 410(10) K for Sb and Co, respectively. The total Debye temperature of $CoSb_3$ from the macroscopic measurement is 280(10) K, which is

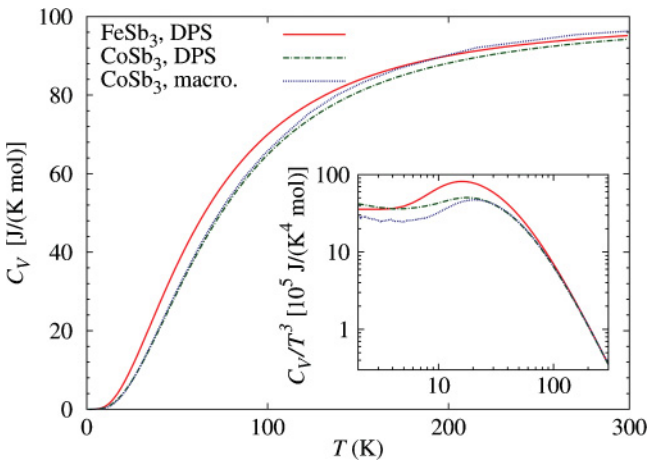

FIG. 10. (Color online) A comparison of the total heat capacity, calculated from the DPS of $FeSb_3$ (red solid lines) and from the DPS and theoretical calculations for $CoSb_3$ (green dash-dotted lines), and the macroscopic measured heat capacity of $CoSb_3$ (blue dotted lines).

in good agreement with the θ_D = 285(10) K obtained from the combined experimental ^{121}Sb NIS C_V and the theoretical Co C_V.

From the Debye level $\lim_{E\to 0}[g(E)/E^2]$, obtained from the low-energy modes in the reduced DPS (see the insets to Fig. 9), the average velocity of sound v_s of 2390(10) and 2790(10) m/s for $FeSb_3$ and $EuFe_4Sb_{12}$, respectively, was obtained from the ^{57}Fe NIS using[47]

$$\lim_{E\to 0}[g(E)/E^2] = \frac{m_R}{2\pi^2\rho\hbar^3 v_s^3}, \quad (1)$$

where ρ is the density of the material and m_R is the mass of the resonant nucleus. These velocities of sound are consistent with the Sb Debye level in $FeSb_3$ and $EuFe_4Sb_{12}$, as indicated by the dashed lines in the insets to Fig. 9; see also Table III. For $CoSb_3$, a v_s of 2600(100) m/s is obtained from the Debye level, which is in fair agreement with the literature value[28] of 2930 m/s. The large error arises from the imprecision in the Debye level obtained only from the ^{121}Sb NIS. By using the low-temperature Debye approximation $v_s = (k_B\theta_D)/[\hbar(6\pi^2 N)^{1/3}]$, with the density of atoms N, the low-temperature θ_D^{LT} = 245(5) K is obtained for $FeSb_3$, a value that is significantly lower than θ_D^{LT} = 307 K reported for $CoSb_3$.[39]

The Lamb-Mössbauer factor f_{LM} obtained from NIS provides access to the atomic mean-square displacements, $\langle u^2\rangle = -\ln(f_{LM})/k^2$, where k is the incident wave vector.[20] In $FeSb_3$, the f_{LM}^{Sb} is 0.58(1) and $\langle u^2\rangle$ is 0.0015(5) Å^2 for Sb at 25 K, and f_{LM}^{Fe} is 0.733(5) and $\langle u^2\rangle$ is 0.0057(4) Å^2 for Fe at 295 K. These values are much smaller than the $\langle u^2\rangle$ values obtained by diffraction. Note that the displacement parameter obtained by NIS is a purely incoherent one-particle displacement and is not affected by the site occupation or disorder, whereas the $\langle u^2\rangle$ values obtained from diffraction sometimes are affected. The temperature dependence of $\langle u^2\rangle$ obtained from the DPS[20] is in agreement with the temperature dependence of $\langle u^2\rangle$ obtained by diffraction, apart from an additive constant, which reflects either a static displacement, a site disorder, or an incomplete site occupation. The element-specific Debye temperatures can also be calculated directly from $g(E)$ with the expression $\theta_D^2 = 3/[k_B^2\int_0^\infty g(E)dE/E^2]$ obtained in the high-temperature limit; see Ref. 20. For $FeSb_3$, Debye temperatures of 210(10) K for Sb and 370(5) K for Fe were obtained; the average value of 255(5) K is in agreement with 245(5) and 240(10) K obtained from sound velocity and C_V, respectively. The element-specific Debye temperature in $CoSb_3$ was obtained from the measured ^{121}Sb DPS of 245(5) K, and from the theoretical Co DPS[16] of 360(10) K. In order to provide an easy comparison between the results of the different methods, we give a summary of all the Debye temperatures in Table III. Arguably, the Debye temperature is a crude approximation, but allows straightforward comparison. In essence, we observe that the Sb sublattice is systematically softer in $FeSb_3$, whereas the Fe sublattice in $FeSb_3$ is harder than the Co sublattice in $CoSb_3$.

The DPS obtained from NIS also directly yields the element-specific mean force constants[20] $F^m = m_R/\hbar\int_0^\infty g(E)E^2dE$. The mean force constant of 160(10) N/m for Sb in $CoSb_3$ is larger than the values of 105(5) and 100(10) N/m observed for $FeSb_3$ and $EuFe_4Sb_{12}$, respectively, because the high-energy optical phonon modes of the filled structure are similar to $FeSb_3$, whereas in $CoSb_3$, they have a larger energy. The Sb force constant in $CoSb_3$ deviates from the literature value of 117 N/m obtained from earlier NIS measurements[17] and from the mean force constant of Sb of 119 N/m obtained from calculations.[16] This deviation can be ascribed essentially to the better resolution and more precise energy calibration available herein.[22] Thus, the good agreement obtained earlier[16,17] is not confirmed herein and the experimental mean force constant in $CoSb_3$ appears to be larger than the calculated value. The Sb mean force constant for $EuFe_4Sb_{12}$ is in good agreement with the F^m obtained from previous NIS measurements.[17] This indicates that by filling $FeSb_3$ with Eu, the average Sb binding does not change. Further, $CoSb_3$ has very different Sb lattice dynamics and thus is not an ideal compound for investigating the influence of filling upon the lattice dynamics of the RFe_4Sb_{12} compounds. In $FeSb_3$, the Fe mean force constant is 186(1) N/m, which is a value close to the value of 190(4) N/m in $EuFe_4Sb_{12}$. The calculated mean force constant[16] for Co in $CoSb_3$ of 176 N/m is slightly smaller, indicating a softer Co binding in the Co_4Sb_{12} framework, as compared to the Fe binding in the Fe_4Sb_{12} framework.

IV. CONCLUSION

The magnetic and electric properties of $FeSb_3$ reveal semiconducting and paramagnetic behavior similar to $CoSb_3$ with, however, a larger effective paramagnetic moment. X-ray diffraction and Mössbauer spectral measurements reveal that the sample is very pure with at most 3 wt.% of elemental Sb as an impurity. Measurements of the lattice dynamics and the related quantities show that the Sb binding in $FeSb_3$ is significantly softer than in $CoSb_3$, whereas the Fe sublattice in $FeSb_3$ is harder compared to the Co sublattice in $CoSb_3$. The softening of the low-energy modes likely has a large influence on the thermal conductivity and thus favorably impacts the thermoelectric properties in $FeSb_3$. By filling the Fe_4Sb_{12} framework, the low-energy optical phonon modes, which have mainly Sb character, shift to larger energies. The lattice dynamics in filled skutterudites depends both on the framework and the filler and, therefore, the Co_4Sb_{12} framework is not ideal for the study of the influence of the filler on the lattice dynamics in RFe_4Sb_{12} skutterudites. It appears that for skutterudites, as was also suggested for clathrates,[48] the role of the framework on the lattice dynamics should be revisited.

ACKNOWLEDGMENTS

We thank Dr. H.-C. Wille and D. Bessas for their support during the NIS measurements and Dr. J. C. Feldman for making his calculation data[16] available. We thank Dr. B. C. Sales for providing the $CoSb_3$ and $EuFe_4Sb_{12}$ samples.[17] The European Synchrotron Radiation Facility and the Advanced Photon Source are acknowledged for provision of synchrotron radiation beam time at the nuclear resonance station ID18 and ID22N and the high-energy station 6-ID-D, respectively. R.H. acknowledges support from the Helmholtz University Young

Investigator Group "Lattice Dynamics in Emerging Functional Materials". F.G. acknowledges the financial support of the Fonds National de la Recherche Scientifique, Belgium (Grants No. 9.456595 and No. 1.5.064.05). The research at the University of Oregon was funded by the National Science Foundation under Grant No. DMR 0907049 and supported in part by ONR Grant No. N00014-07-1-0358 and by the Army Research Laboratory under Agreement No. W911NF-07-2-0083.

*r.hermann@fz-juelich.de

[1] J. P. Fleurial, T. Caillat, and A. Borshchevsky, AIP Conf. Proc. **316**, 40 (1995).
[2] B. C. Sales, D. Mandrus, B. C. Chakoumakos, V. Keppens, and J. R. Thompson, Phys. Rev. B **56**, 15081 (1997).
[3] G. S. Nolas, D. T. Morelli, and T. M. Tritt, Annu. Rev. Mater. Sci. **29**, 89 (1999).
[4] C. Uher, Semicond. Semimet. **69**, 139 (2001).
[5] G. S. Nolas, G. A. Slack, D. T. Morelli, T. M. Tritt, and A. C. Ehrlich, J. Appl. Phys. **79**, 4002 (1995).
[6] G. S. Nolas, J. L. Cohn, and G. A. Slack, Phys. Rev. B **58**, 164 (1998).
[7] G. P. Meisner, D. T. Morelli, S. Hu, J. Yang, and C. Uher, Phys. Rev. Lett. **80**, 3551 (1998).
[8] J. L. Feldman and D. J. Singh, Phys. Rev. B **53**, 6273 (1996).
[9] V. Keppens, D. Mandrus, B. C. Sales, B. C. Chakoumakos, P. Dai, R. Coldea, M. B. Maple, D. A. Gajewski, E. J. Freeman, and S. Bennington, Nature (London) **395**, 876 (1998).
[10] R. P. Hermann, R. Jin, W. Schweika, F. Grandjean, D. Mandrus, B. C. Sales, and G. J. Long, Phys. Rev. Lett. **90**, 135505 (2003).
[11] M. M. Koza, M. R. Johnson, R. Viennois, H. Mutka, L. Girard, and D. Ravot, Nature Mater. **7**, 805 (2008).
[12] M. Rotter, P. Rogl, A. Grytsiv, W. Wolf, M. Krisch, and A. Mirone, Phys. Rev. B **77**, 144301 (2008).
[13] B. C. Sales, B. C. Chakoumakos, and D. Mandrus, Phys. Rev. B **61**, 2475 (2000).
[14] C. Uher, *Thermoelectrics Handbook: Macro to Nano* (Taylor & Francis, Boca Raton, 2006).
[15] J. Yang, Q. Hao, H. Wang, Y. C. Lan, Q. Y. He, A. Minnich, D. Z. Wang, J. A. Harriman, V. M. Varki, M. S. Dresselhaus, G. Chen, and Z. F. Ren, Phys. Rev. B **80**, 115329 (2009).
[16] J. L. Feldman, P. Dai, T. Enck, B. C. Sales, D. Mandrus, and D. J. Singh, Phys. Rev. B **73**, 014306 (2006).
[17] H.-C. Wille, R. P. Hermann, I. Sergueev, O. Leupold, P. van der Linden, B. C. Sales, F. Grandjean, G. J. Long, R. Rüffer, and Yu. V. Shvyd'ko, Phys. Rev. B **76**, 140301(R) (2007).
[18] M. D. Hornbostel, E. J. Hyer, J. Thiel, and D. C. Johnson, J. Am. Chem. Soc. **119**, 2665 (1997).
[19] J. R. Williams, M. B. Johnson, and D. C. Johnson, J. Am. Chem. Soc. **123**, 1645 (2001).
[20] R. Rüffer and A. I. Chumakov, Hyperfine Interact. **128**, 225 (2000).
[21] W. Sturhahn, T. S. Toellner, E. E. Alp, X. Zhang, M. Ando, Y. Yoda, S. Kikuta, M. Seto, C. W. Kimball, and B. Dabrowski, Phys. Rev. Lett. **74**, 3832 (1995); M. Seto, Y. Yoda, S. Kikuta, X. W. Zhang, and M. Ando, *ibid.* **74**, 3828 (1995).
[22] I. Sergueev, H.-C. Wille, R. P. Hermann, D. Bessas, Y. V. Shvyd'ko, M. Zajac, and R. Rüffer, J. Synch. Rad. **18**, (2011).
[23] M. Noh, J. Thiel, and D. C. Johnson, Science **270**, 1181 (1995).
[24] A. P. Hammersley, *FIT2D: An Introduction and Overview* (ESRF Internal Report, ESRF97HA02T, 1997).
[25] J. Rodriguez-Carvajal, computer code FULLPROF V [Laboratoire Leon Brillouin (CEA-CNRS), France, 2009].
[26] D. Mandrus, A. Migliori, T. W. Darling, M. F. Hundley, E. J. Peterson, and J. D. Thompson, Phys. Rev. B **52**, 4926 (1995).
[27] H. Anno, K. Hatada, H. Shimizu, K. Matsubara, Y. Notohara, T. Sakakibara, H. Tashiro, and K. Motoya, J. Appl. Phys. **83**, 5270 (1998).
[28] T. Caillat, A. Borshchevsky, and J. P. Fleurial, J. Appl. Phys. **80**, 4442 (1996).
[29] L. D. Chen, T. Kawahara, X. F. Tang, T. Goto, T. Hirai, J. S. Dyck, W. Chen, and C. Uher, J. Appl. Phys. **90**, 1864 (2001).
[30] M. Puyet, B. Lenoir, A. Dauscher, P. Pécheur, C. Bellouard, J. Tobola, and J. Hejtmanek, Phys. Rev. B **73**, 035126 (2006).
[31] A. L. E. Smalley, S. Kim, and D. C. Johnson, Chem. Mater. **15**, 3847 (2003).
[32] J. Yang, G. P. Meisner, D. T. Morelli, and C. Uher, Phys. Rev. B **63**, 014410 (2000).
[33] J. Yang, M. G. Endres, and G. P. Meisner, Phys. Rev. B **66**, 014436 (2002).
[34] T. Rosenqvist, Acta Metall. **1**, 761 (1953).
[35] G. Rogl, L. Zhang, P. Rogl, A. Grytsiv, M. Falmbigl, D. Rajs, M. Kriegisch, H. Müller, E. Bauer, J. Koppensteiner, W. Schranz, M. Zehetbauer, Z. Henkie, and M. B. Maple, J. Appl. Phys. **107**, 043507 (2010).
[36] L. Zhang, G. Rogl, A. Grytsiv, S. Puchegger, J. Koppensteiner, F. Spieckermann, H. Kabelka, M. Reinecker, P. Rogl, W. Schranz, M. Zehetbauer, and M. A. Carpenter, Mater. Sci. Eng. B **170**, 26 (2010).
[37] D. T. Morelli, V. Jovovic, and J. P. Heremans, Phys. Rev. Lett. **101**, 035901 (2008).
[38] B. T. M. Willis and A. W. Pryor, *Thermal Vibrations in Crystallography* (Cambridge University Press, Cambridge, 1975).
[39] R. P. Hermann, F. Grandjean, and G. J. Long, Am. J. Phys. **73**, 110 (2005).
[40] B. C. Chakoumakos and B. C. Sales, J. Alloys Compd. **407**, 87 (2006).
[41] R. H. Herber in *Chemical Mössbauer Spectroscopy*, edited by R. H. Herber (Plenum, New York, 1984), p. 199.
[42] G. K. Shenoy and F. E. Wagner, *Mössbauer Isomer Shifts* (North-Holland, Amsterdam, 1978) p. 49.
[43] T. Owen, F. Grandjean, G. J. Long, K. V. Domasevitch, and N. Gerasimchuk, Inorg. Chem. **47**, 8704 (2008).
[44] V. G. Kohn and A. I. Chumakov, Hyperfine Interact. **125**, 205 (2000).
[45] H. J. Lipkin, Phys. Rev. B **52**, 10073 (1995).
[46] G. J. Long, R. P. Hermann, F. Grandjean, E. E. Alp, W. Sturhahn, C. E. Johnson, D. E. Brown, O. Leupold, and R. Rüffer, Phys. Rev. B **71**, 140302 (2005).
[47] M. Y. Hu, W. Sturhahn, T. S. Toellner, P. D. Mannheim, D. E. Brown, J. Zhao, and E. E. Alp, Phys. Rev. B **67**, 094304 (2003).
[48] M. Christensen, A. B. Abrahamsen, N. B. Christensen, F. Juranyi, N.H. Andersen, K. Lefmann, J. Andreasson, C. R. H. Bahl, and B. B. Iversen, J. Am. Chem. Soc. **128**, 15657 (2006).